Supporting Information

Moerman et al. 10.1073/pnas.1716330115

Model Specification and Energetics

The instantaneous concentrations of oil, water, and ethanol at a given location within the domain are denoted by $c_o = c_o(\boldsymbol{x}, t)$, $c_w = c_w(\boldsymbol{x}, t)$, and $c_e = c_e(\boldsymbol{x}, t)$, respectively. Since ethanol is as miscible in oil as it is in water or in a mixture of both, it is sensible to describe oil and water as a binary mixture, with ethanol viewed as a spatiotemporal control parameter acting on this mixture. Without loss of generality, we can focus on the relative concentration of water to oil, $\phi(\boldsymbol{x}, t)$, defined as

$$\phi(\boldsymbol{x}, t) = \frac{c_w(\boldsymbol{x}, t) - c_o(\boldsymbol{x}, t)}{c_w(\boldsymbol{x}, t) + c_o(\boldsymbol{x}, t)} \qquad \textbf{[S1]}$$

so that $\phi(\boldsymbol{x}, t) = +1$ if $c_o(\boldsymbol{x}, t) = 0$ (pure water) and $\phi(\boldsymbol{x}, t) = -1$ if $c_w(\boldsymbol{x}, t) = 0$ (pure oil). To account for the energetics of the mixture, we use a ϕ^4-type Ginzburg–Landau energy functional

$$E[\phi; c_e] = \int_\Omega \left(\tfrac{1}{2}\gamma^2 |\nabla\phi(\boldsymbol{x}, t)|^2 + \tfrac{1}{2} f(c_e(\boldsymbol{x}, t))\phi^2(\boldsymbol{x}, t) + \tfrac{1}{4}\phi^4(\boldsymbol{x}, t)\right) d\boldsymbol{x} \qquad \textbf{[S2]}$$

Here ∇ denotes the gradient operator, and $\Omega \in \mathbb{R}^3$ is the domain (i.e., the sphere of radius R for the droplet, and the semiinfinite cylinder of radius R for the capillary). The energy (Eq. **S2**) contains two contributions: The first comes from the exchange (or interfacial) energy term $\frac{1}{2}\gamma^2|\nabla\phi(\boldsymbol{x}, t)|^2$, with γ being a parameter with the unit of a length that controls the width of the interface between oil and water in the regions where they are immiscible. The second comes from the potential term $\frac{1}{2} f(c_e(\boldsymbol{x}, t))\phi^2(\boldsymbol{x}, t) + \frac{1}{4}\phi^4(\boldsymbol{x}, t)$ that controls the miscibility of the mixture of water and oil at a given concentration of ethanol: In particular, $f(c_e(\boldsymbol{x}, t)) > 0$ if $c_e(\boldsymbol{x}, t) > c_\star \approx 0.469$ (this value is based on the experimental data) so that the potential has a single well, indicating that oil and water are miscible, whereas $f(c_e(\boldsymbol{x}, t)) < 0$ if $c_e(\boldsymbol{x}, t) < c_\star$, so that the potential has a double well, indicating that oil and water are immiscible (see Fig. S5 for an illustration). Several choices for the function $f(c_e)$ are possible: In the main text, we took the simplest one and assumed that $f(c_e(\boldsymbol{x}, t)) = +1$ in the miscible region where $c_e(\boldsymbol{x}, t) > c_\star$ and $f(c_e(\boldsymbol{x}, t)) = -1$ in the immiscible region where $c_e(\boldsymbol{x}, t) < c_\star$. Another possibility, used in Fig. S5 for illustration of the phase diagram, is to take $f(c_e(\boldsymbol{x}, t)) = \tanh(\alpha(c_e(\boldsymbol{x}, t) - c_\star))$ for some $\alpha > 0$.

Dynamics

Within a ϕ^4 field-theoretic description, the driving force for the dynamics of $\phi(\boldsymbol{x}, t)$ is the chemical potential, defined as the functional derivative of $E[\phi; c_e]$ with respect to $\phi(\boldsymbol{x}, t)$. It is given by

$$\mu(\boldsymbol{x}, t) \equiv \frac{\delta E[\phi; c_e]}{\delta\phi(\boldsymbol{x}, t)} = -\gamma^2\Delta\phi(\boldsymbol{x}, t) + f(c_e(\boldsymbol{x}, t))\phi(\boldsymbol{x}, t) + \phi^3(\boldsymbol{x}, t) \qquad \textbf{[S3]}$$

where Δ denotes the Laplacian. The dynamics of $\phi(\boldsymbol{x}, t)$ must also be conservative—that is, such that $\int_\Omega (\phi(\boldsymbol{x}, t) - \phi(\boldsymbol{x}, 0))\, d\boldsymbol{x} = 0$, which requires mass transport within the domain upon phase separation. Different evolution equations can be derived depending on the way this mass transport occurs. The standard CH equation is obtained by assuming that mass transport is diffusive, which implies that the rate of change of $\phi(\boldsymbol{x}, t)$ is proportional to the Laplacian of $\mu(\boldsymbol{x}, t)$, that is

$$\begin{aligned}\partial_t\phi(\boldsymbol{x}, t) &= D_\phi\Delta\mu(\boldsymbol{x}, t)\\ &= -D_\phi\Delta\left(\gamma^2\Delta\phi(\boldsymbol{x}, t) - f(c_e(\boldsymbol{x}, t))\phi(\boldsymbol{x}, t) - \phi^3(\boldsymbol{x}, t)\right)\end{aligned} \qquad \textbf{[S4]}$$

where D_ϕ is a diffusion coefficient. Eq. **S4** should be solved with a no-flux boundary condition at the boundary of the domain, $\partial\Omega$. Similarly, the mass-conserving Allen–Cahn equation (Eq. **2**) is obtained by assuming that mass transport is quasi-instantaneous within the domain, which implies that the rate of change of $\phi(\boldsymbol{x}, t)$ is proportional to $-\mu(\boldsymbol{x}, t)$ minus its average; that is

$$\begin{aligned}\partial_t\phi(\boldsymbol{x}, t) = -\tau^{-1}(\mu(\boldsymbol{x}, t) - \bar{\mu}(t)) = \tau^{-1}\left(\gamma^2\Delta\phi(\boldsymbol{x}, t)\right.\\ \left. - f(c_e(\boldsymbol{x}, t))\phi(\boldsymbol{x}, t) - \phi^3(\boldsymbol{x}, t) + \bar{\mu}(t)\right)\end{aligned} \qquad \textbf{[S5]}$$

where τ is a characteristic relaxation time and $\bar{\mu}(t)$ is given by the spatial average of $\mu(\boldsymbol{x}, t)$ over the domain

$$\begin{aligned}\bar{\mu}(t) = V_\Omega^{-1}\int_\Omega \mu(\boldsymbol{x}, t)\, d\boldsymbol{x} = -V_\Omega^{-1}\int_\Omega \left(f(c_e(\boldsymbol{x}, t))\phi(\boldsymbol{x}, t)\right.\\ \left. + \phi^3(\boldsymbol{x}, t)\right) d\boldsymbol{x}\end{aligned} \qquad \textbf{[S6]}$$

Here V_Ω is the volume of the domain Ω, and we used the no-flux boundary condition on $\partial\Omega$ to get rid of the integral of $\gamma^2\Delta\phi(\boldsymbol{x}, t)$. The term $\bar{\mu}(t)$ can be thought of as a Lagrange multiplier term added to enforce the constraint of mass conservation. In the main text, we used Eq. **S5** to describe phase separation in the droplets, which amounts to assuming that the excess mass of oil or water created by phase separation is transported toward the center of the droplet much faster than the immiscibility front progresses in this domain. While this assumption is consistent with the observations in the finite-size droplets, it is not valid in the capillary whose elongation is too large to allow for quasi-instantaneous transport all across. This is why we modified Eq. **S5** into

$$\begin{aligned}\partial_t\phi(\boldsymbol{x}, t) = -\tau^{-1}(\mu(\boldsymbol{x}, t) - \langle\mu\rangle_{B(t)}) = \tau^{-1}\left(\gamma^2\Delta\phi(\boldsymbol{x}, t)\right.\\ \left. - f(c_e(\boldsymbol{x}, t))\phi(\boldsymbol{x}, t) - \phi^3(\boldsymbol{x}, t) + \langle\mu\rangle_{B(t)}\right)\end{aligned} \qquad \textbf{[S7]}$$

if $\boldsymbol{x} \in B(t)$ and $\partial_t\phi(\boldsymbol{x}, t) = 0$ otherwise—this is Eq. **5**. Here $\langle\mu\rangle_{B(t)}$ denotes the spatial average of $\mu(\boldsymbol{x}, t)$ in the domain $B(t) \subseteq \Omega$ that only extends a phenomenological length L ahead of the immiscibility front separating the regions where $f(c_e) = +1$ and $f(c_e) = -1$ in Ω. Explicitly $B(t)$ is defined via

$$\boldsymbol{x} \in B(t) \quad \text{if} \quad \min_{\substack{\boldsymbol{y} \text{ such that}\\ c_e(\boldsymbol{y}, t) \geq c_\star}} |\boldsymbol{x} - \boldsymbol{y}| \leq L \qquad \textbf{[S8]}$$

or, equivalently, $\boldsymbol{x} \in B(t)$ if there exists a $\boldsymbol{x}$ such that $c_e(\boldsymbol{y}, t) \geq c_\star$ and $|\boldsymbol{y} - \boldsymbol{x}| \leq L$, and $\langle\mu\rangle_{B(t)}$ is given by

$$\begin{aligned}\langle\mu\rangle_{B(t)} &= V_{B(t)}^{-1}\int_{B(t)} \mu(\boldsymbol{x}, t)\, d\boldsymbol{x}\\ &= -V_{B(t)}^{-1}\int_{B(t)} \left(f(c_e(\boldsymbol{x}, t))\phi(\boldsymbol{x}, t) + \phi^3(\boldsymbol{x}, t)\right) d\boldsymbol{x}\end{aligned} \qquad \textbf{[S9]}$$

where $V_{B(t)}$ is the volume of the domain $B(t)$. Eq. **S7** should be solved with the condition $\phi(\boldsymbol{x}, t) = \phi(\boldsymbol{x}, 0)$ for $\boldsymbol{x} \in \partial B(t)$, and it is easy to see that this equation implies mass conservation because

$$\frac{d}{dt}\int_{B(t)}(\phi(\boldsymbol{x},t)-\phi(\boldsymbol{x},0))\,d\boldsymbol{x}=\int_{B(t)}\partial_t\phi(\boldsymbol{x},t)\,d\boldsymbol{x}$$
$$=-\tau^{-1}\int_{B(t)}(\mu(\boldsymbol{x},t)-\langle\mu\rangle_{B(t)})\,d\boldsymbol{x} \qquad \textbf{[S10]}$$
$$=-\tau^{-1}V_{B(t)}(\langle\mu\rangle_{B(t)}-\langle\mu\rangle_{B(t)})=0$$

where we got the first equality by using the fact that $\phi(\boldsymbol{x},t)=\phi(\boldsymbol{x},0)$ for $\boldsymbol{x}\in\partial B(t)$.

Notice that if L is larger than the domain size (e.g., $L>R$ in the case of the droplets), then $B(t)$ coincides the whole domain (i.e., $\Omega\equiv B(t)$ for all $t\geq 0$) and Eq. **S7** reduces to Eq. **S5**. Notice also that if the interfacial length γ is very small compared with the domain size, then on the time scale over which the ethanol sips out and the layers are created, we can drop the exchange terms in Eqs. **S5** and **S7**. Finally, notice that while the results reported in main text are sensitive to the value of τ, they are not to that of L as long as this length remains larger than the size of the layers.

It should be stressed that all three models above—that is, Eqs. **S4**, **S5**, and **S7**—are phenomenological, and their validity should therefore be assessed in function of their ability to reproduce the experimental data at hand. In the context of the experiments we describe in main text, Eq. **S5** and, more generally, Eq. **S7** were clearly adequate models. We believe that Eq. **S7** could also be useful in other contexts. Interestingly, this equation has the added advantage of being simpler to analyze and integrate numerically than the standard CH equation, because (*i*) Eq. **S7** only involves second-order derivatives, whereas Eq. **S4** involves fourth-order spatial derivatives that make it very stiff, and (*ii*) it is easier to take the sharp interface limit on Eq. **S7** than on Eq. **S4**, because Eq. **S7** remains well-posed if we set $\gamma=0$ in this equation, whereas Eq. **S4** does not.

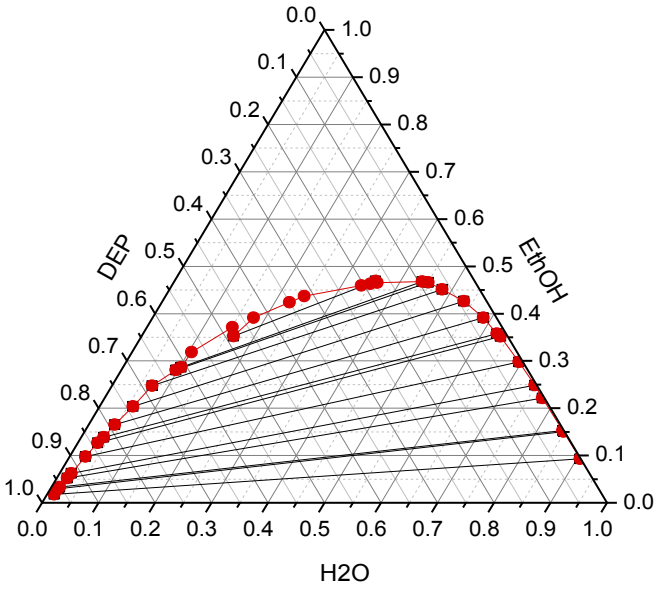

Fig. S1. Ternary phase diagram for the mixture of DEP, water, and ethanol, obtained experimentally by bulk titration.

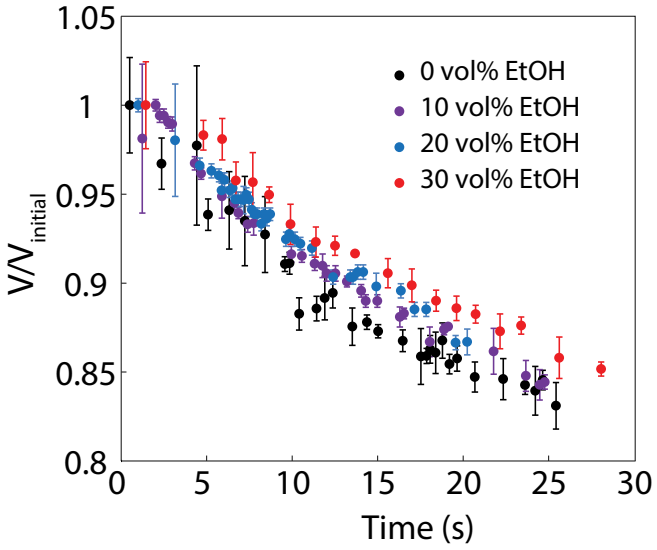

Fig. S2. Droplet shrinkage in terms of the ratio of the droplet volume V scaled by the initial volume $V_{initial}$, as the ethanol leaks out. The legend shows data for varying concentrations of ethanol on the outside of the droplet, which slows down the leakage rate.

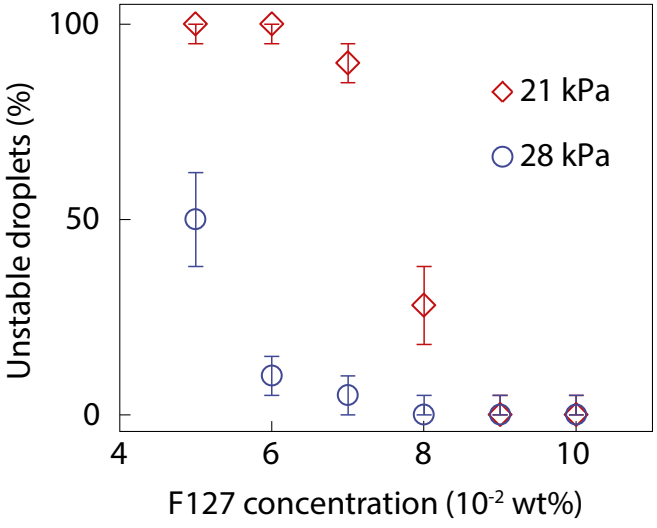

Fig. S3. Percentage of droplets that have released their inner layers after half an hour of waiting time, as a function of the surfactant concentration and flow rate of the continuous phase. Note that the number of stable droplets strongly depends on surfactant concentration. The legend gives applied pressure that sets the flow rate in the outer microfluidic channel. The ratio between inner and outer flow rate also affects the surfactant concentration and by extension the fraction of stable droplets.

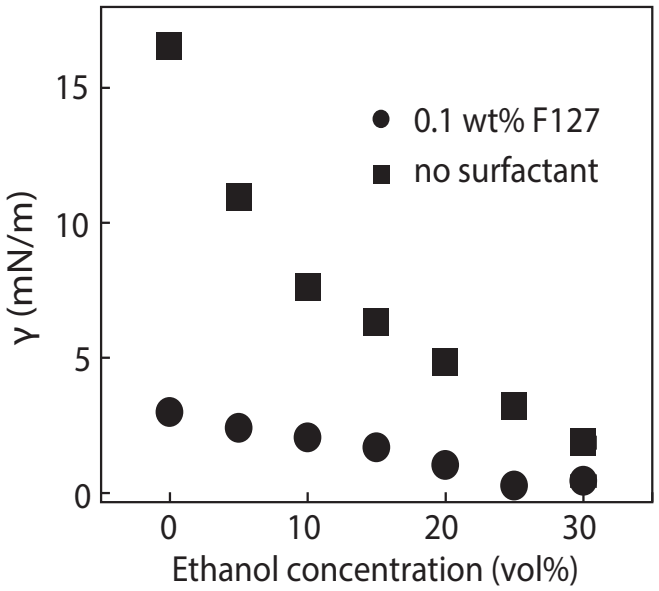

Fig. S4. Interfacial tension between DEP oil and water decreases with ethanol content, with or without surfactant. Through diffusiophoresis, this drives the droplets nucleated by phase separation toward the center, where ethanol concentration is the highest.

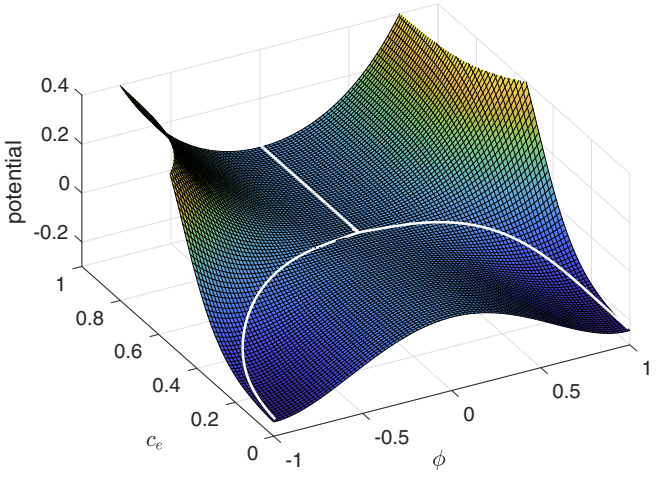

Fig. S5. 3D plot of the potential $\frac{1}{2}f(c_e)\phi^2 + \frac{1}{4}\phi^4$ with $f(c_e) = \tanh(5(c_e - c_\star))$. The white line shows the spinodal line.

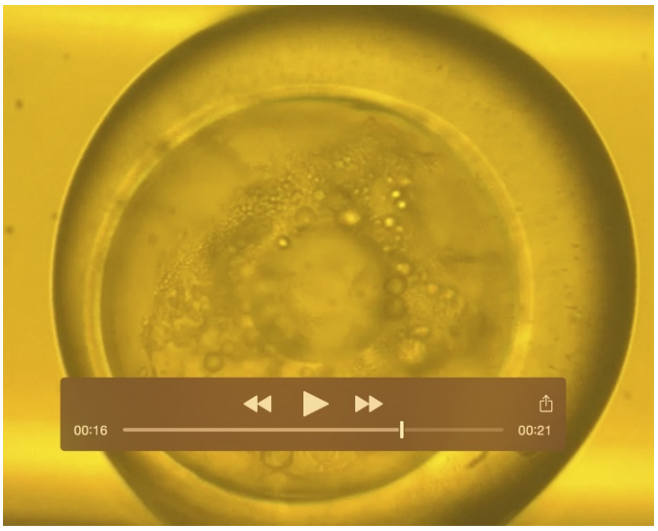

Movie S1. The formation of a multiple emulsion droplet from the phase separation of a ternary mixture of water:DEP:ethanol (0.15:0.47:0.38) in a microfluidic droplet of 150 μm in radius suspended in a continuous phase of 0.1 wt% of F127 surfactant. The movie shows the mechanism of layer formation, emphasizing the faster-than-diffusive mixing and the radial scooping of droplets toward the center due to Marangoni forces. Snapshots are shown in Fig. 1. The jitter is due to the camera chasing the droplet downstream as it leaves the micropipette tip.

Movie S1

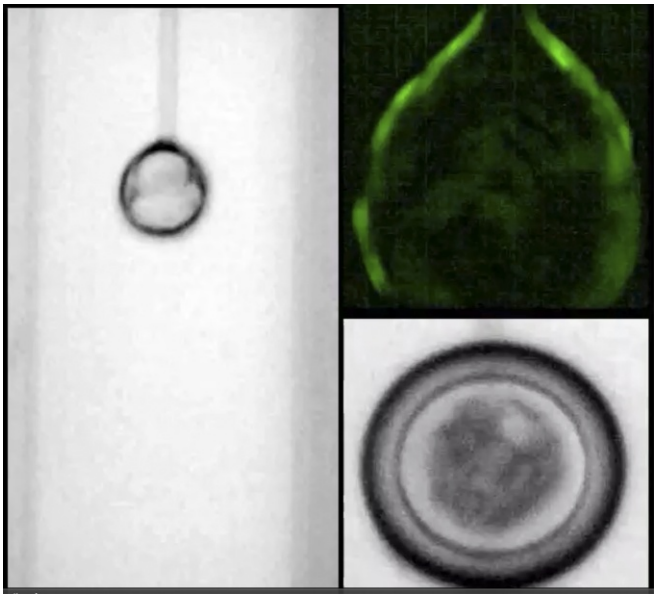

Movie S2. Formation of a quintuple emulsion from the phase separation of a ternary mixture of water, DEP, and ethanol in a microfluidic droplet of 50 μm in radius, slowed down by polyalginate in the aqueous phase. *Top* panel shows the oil phase dyed with Nile Red, and the *Bottom* panel shows the movie such that the droplet is in the center of the frame. This droplet is similar to the one presented in Fig. 2*iii*.

Movie S2

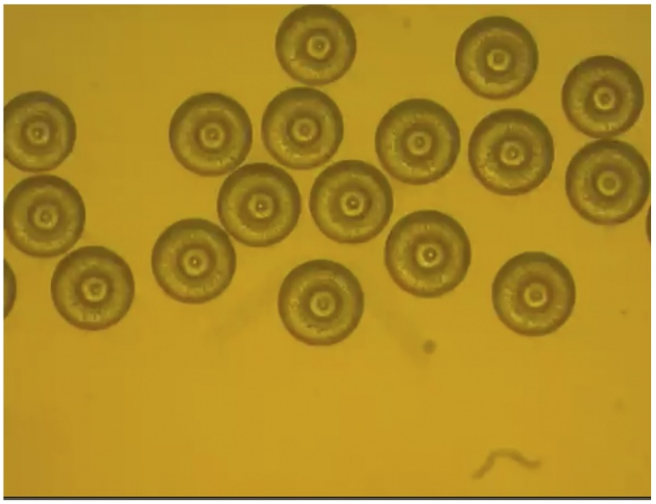

Movie S3. Timed-release of inner layers of a multiple emulsion made from a water:DEP:ethanol (0.15: 0.47: 0.38) mixture in the presence of 0.01 wt% F127 surfactant. The movie shows the stepwise release of the inner layers of oil into the continuous phase. The movie is in real time and generates data shown in Fig. 4.

Movie S3

Movie S4. Movie of the phase separation process of a ternary mixture of water:DEP:ethanol (0.15:0.47:0.38) inside a rectangular capillary, dipped into the aqueous phase containing 0.1 wt% of F127 surfactant on the edge seen on the right hand side. The frames are separated by 20 min, so the movie has been sped up 600 times. Snapshots of this movie are shown in Fig. 5*A*.

Movie S4

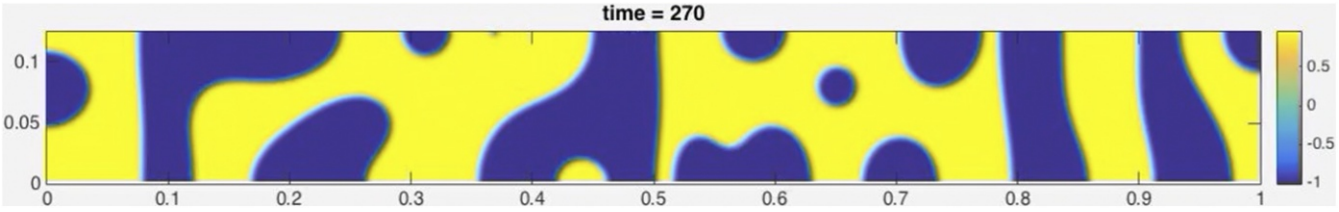

Movie S5. In the model, as in the experiments, if the quench takes place homogeneously throughout the capillary, phase separation occurs by standard spinodal decomposition. In this regime, the behavior of the solutions to the nonlocal conservative Allen–Cahn Eq. **2** is qualitatively similar to that of the classical CH equation. The capillary *xy* scale is shown in centimeters, and the color map corresponds to the relative concentration of water to oil $\phi(x, t)$.

Movie S5

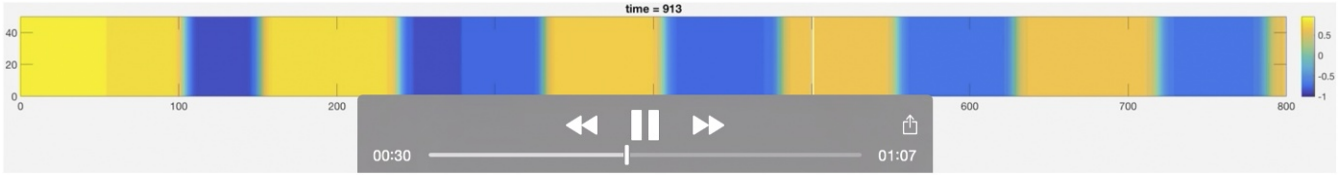

Movie S6. A diffusive front driving the phase separation in Eq. **5** reproduces the experimental dynamics of the formation of stripe patterns of the oil-rich (yellow) and the water-rich (blue) regions from the edge of the capillary (on the left) inwards. The capillary *xy* scale is shown in μm, and the color map corresponds to the relative concentration of water to oil $\phi(x, t)$.

Movie S6